RSC Advances

RSC Publishing

PAPER

View Article Online
View Journal | View Issue

Cite this: *RSC Advances*, 2013, **3**, 13843

Structural properties and electrochemical behavior of cone-like TiO_2: emphasizing the contributions of structure and spatial arrangement to lithium storage

Jianfei Lei,*[a] Kai Du,[a] Ronghui Wei,[a] Jing Ni,[a] Liben Li[a] and Weishan Li*[bcd]

Received 4th April 2013,
Accepted 13th May 2013

DOI: 10.1039/c3ra41624k

www.rsc.org/advances

A novel structure of anatase TiO_2, nanocone-like TiO_2 (TiO_2-NC), is successfully prepared by a simple liquid-phase deposition method and is used as an anode material. The morphology and spatial arrangement of the TiO_2-NC greatly affects the lithium storage, and TiO_2-NC achieves a sustained high lithium storage performance (254.7 mA h g^{-1}, corresponding to $Li_{0.76}TiO_2$) by assembling the TiO_2-NC into ordered spherical shells. The structural analysis shows that exposed {001} facets of nanosized TiO_2-NC help to increase the surface area as well as shorten the diffusion path of lithium transport. Moreover, an ordered arrangement of the TiO_2-NC with a channel structure can further increase the surface area and improve the diffusion of the electrolyte, hence enhancing the lithium storage. Electrochemical tests indicate that the bulk intercalation of lithium was accompanied by the phenomenon of interfacial lithium storage in the TiO_2-NC. In addition, the polarization of the TiO_2-NC hollow spheres is effectively inhibited due to the ordered structure providing comfortable channels for the ionic and electronic diffusion, which imparts improved rate performance.

Introduction

In the last decade, substantial efforts have been made to develop advanced lithium ion batteries (LIB) with higher storage capacities and power densities for applications in high-performance portable devices and hybrid electric vehicles (HEV).[1–7] In principle, energy storage in the form of LIB requires insertion of lithium metal into host materials. In order to improve the kinetics of such storage reactions, nanostructuring of the material has proven to be a promising strategy by shortening the diffusion paths for electrolyte contacting host materials, as well as influencing both ionic and electronic charge transport relevant to electrochemical processes.[8–10] In addition, nanosized materials can provide high porosity and a large surface area, thus excess lithium can be accommodated at the interfaces of the nanosized particles in a composite electrode system (not only at the solid–liquid interface, but also at the solid–solid interface between the lithium host materials, the electrolyte, and the conductive additives), resulting in an increase of the total amount of lithium stored. Therefore, many attempts have been made to synthesize hierarchical, porous, nanosized electrode materials (*e.g.* carbon, silicon, tin and transition-metal oxides), and to utilize them in LIB applications as anode materials.

Titanium dioxide (TiO_2) has attracted much attention for its promising applications in LIB due to its better structure stability and higher lithium insertion potential ($\sim$1.5 V *vs.* Li^+/Li) than carbon materials, thus providing LIB with excellent cycle performance.[11,12] In addition, titanium is abundant in nature and nontoxic. Therefore, various polymorphs of TiO_2, such as rutile, anatase, and TiO_2 (B), have recently been studied as electrode materials for LIB, showing improved lithium-storage properties.[13] Practical applications of TiO_2 for LIB, however, still present a challenge due to the low chemical diffusivity of lithium in TiO_2, which is rate-determining for the lithium incorporation and extraction reactions, although promising electrode systems have recently been proposed. Earlier studies demonstrated that the highly-active {001} facets of anatase TiO_2 provide unusual opportunities for electrochemical energy storage.[14] To exploit the activity of anatase TiO_2 microcrystals with exposed {001} facets,[15] a series of studies have been performed for the synthesis of sheet-like anatase TiO_2 with exposed {001} facets (TiO_2 nanosheets).[16–19] However, the formation of the nanosheets should be carried out in a special reactor (autoclave) and the final product is usually a powder, which limits its applications. In our previous

[a]*School of Physics and Engineering, Henan University of Science and Technology, Luoyang, China. E-mail: leijianfei9966@163.com; Fax: +86379 65626265; Tel: +86379 65626265*
[b]*School of Chemistry and Environment, South China Normal University, Guangzhou, China. E-mail: liwsh@scnu.edu.cn; Fax: +8620 39310256; Tel: +8620 39310256*
[c]*Key Laboratory of Electrochemical Technology on Energy Storage and Power Generation of Guangdong Higher Education Institutes, South China Normal University, Guangzhou, China*
[d]*Engineering Research Center of Materials and Technology for Electrochemical Energy Storage (Ministry of Education), South China Normal University, Guangzhou, China*

report, we prepared cone-like anatase TiO_2 (TiO_2-NC) with exposed {001} facets through a convenient process and assembled them into hollow spheres through polymeric templating.[4] With this technology, we can provide various forms of TiO_2-NC, such as powders, films and supports. We have used the TiO_2-NC as the support of tin oxide nanoparticles to develop a novel anode composite for LIB, which exhibits excellent performance.[4] In addition, TiO_2 films with TiO_2-NC spherical shells currently also show exciting lithium-storage performance. Electrochemical characterizations show that the TiO_2-NCs exhibit excellent performance in terms of enhanced lithium storage properties (203 mA h g^{-1} at 1C) compared to TiO_2 nanospindles (166 mA h g^{-1} at 1C)[20] and improved rate capability (245, 203 and 165 mA h g^{-1} at 1/2, 1 and 2 C) compared to porous TiO_2 (183, 164 and 135 mA h g^{-1} at 1/10, 1 and 2 C).[21]

Compared to normal morphologies, the superior performance of TiO_2-NC stimulates our interest to further investigate its hidden mysteries. In fact, the chemical diffusivity of lithium in TiO_2 mostly depends on two major transport processes: the electronic conductivity of TiO_2 and the diffusivity of Li^+ in the TiO_2 (ambipolar transport). The main efforts to improve the electronic conductivity have been done mainly by adding conductive secondary phases, such as conductive carbons, and RuO_2.[22] On the other hand, the reduction of the TiO_2 particle size is key to improved Li^+-diffusion, rather than electron transport, due to the shorter Li^+-diffusion length for filling the particles. Hence, nanostructuring has largely been studied in LIB because of its greatly improved storage capacity, as well as its rate capability.[23,24] Even further improvement can be achieved with nanostructured materials by introducing a high porosity, large surface area and highly-active facets. Due to the increased impact of both the surface and the interface in nanosized materials, interfacial lithium-storage can play an important role in nanostructured materials beyond the conventional bulk intercalation of lithium into a TiO_2 lattice.

In this paper, we show the structural properties and electrochemical behavior of disordered TiO_2-NC and systematically arranged TiO_2-NC that allow fundamental understanding of the impact of the morphology and spatial arrangement of the TiO_2-NC on the kinetics of lithium insertion/extraction. Anatase TiO_2 is a typical lithium insertion compound, showing strong particle structure-dependent electrochemistry and insertion capacity, hence offering an excellent base for the understanding of the effect of morphology and arrangement on insertion reactions. This provided the motivation to embark on a structure-dependent study of lithium insertion in anatase TiO_2, thus expanding the applications and improving the performance of TiO_2.

Experimental section

Materials synthesis

A freshly prepared liquid-phase deposition (LPD) solution (100 ml) containing $(NH_4)_2[TiF_6]$ (0.05 mol L^{-1}) and H_3BO_3 (0.05 mol L^{-1}), whose pH value was adjusted to 2.9 by adding HCl (2 mol L^{-1}), was kept in a polypropylene beaker. Then the LPD solution was incubated at 50 °C for 8 h. After the reaction, the deposition solution was filtered, and the samples were washed with water and dried at room temperature before further being calcined at 450 °C in an oven for 3 h to obtain cone-like anatase TiO_2 (TiO_2-NC) powders.

Based on the method of polystyrene spheres (PS) functionalization, the polyelectrolyte-coated PS (100 mg) was added to the freshly prepared LPD solution (100 ml, as above described) and was then also incubated at 50 °C for 8 h. After the reaction, the deposition solution was filtered, and the samples were washed with water and dried at room temperature before being dispersed in toluene (100 ml) to remove the PS templates, leaving hollow spheres. Finally, the samples were calcined at 450 °C in an oven for 3 h to obtain TiO_2-NCs hollow spheres powders.

Materials characterization

The morphology of the sample was examined by field-emission scanning electron microscopy (FE-SEM; ZEISS Ultra, Germany) and transmission electron microscopy (TEM; JEM-2100HR, Japan). Crystallographic information for the sample was investigated with X-ray powder diffraction (XRD; Bruker D8 Advance, Germany). The surface area of the sample was measured using a Micromeritics ASAP 2020-physisorption analyzer (USA).

Electrochemical measurements

The electrochemical measurements were carried out using a coin-type cell (CR2025) with a metallic lithium foil as the counter and reference electrodes. The working electrode was the as-prepared samples (TiO_2-NCs or TiO_2-NCs hollow spheres) and the electrolyte was $LiPF_6$ (1.0 mol L^{-1}) in a 1 : 1 (w/w) mixture of ethylene carbonate (EC) and dimethyl carbonate (DMC). Cyclic voltammetry was conducted on a Solartron Analylical 1470E CellTest System (England) at a 0.2 mV s^{-1} scanning rate and the charge/discharge tests were performed using a LAND CT2001A (China) battery testing system at different current rates with a potential window of 1.5–2.5 V (*vs.* Li^+/Li).

Results and discussion

Our anatase TiO_2-NC is obtained by calcining the samples at 450 °C in the oven. The high crystallinity and phase purity of the resultant material are confirmed by X-ray diffraction (XRD, Fig. 1). It can be seen from Fig. 1 that all the main diffraction peaks can be indexed to the anatase crystal phase (space group *I*41/amd, JCPDS No. 21-1272), and no impurity peaks, such as rutile and TiO_2 (B), can be detected. Moreover, remarkably

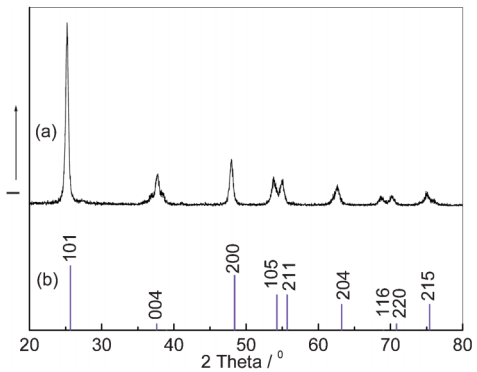

Fig. 1 The XRD pattern of TiO_2 calcined at 450 °C for 3 h.

enhanced (101) and (004) peaks indicate that the TiO_2-NC is dominated by {101} and {001} facets.[25]

As an approach to identify the surface area, pore size and the extent of porosity, the nitrogen adsorption–desorption isotherm was recorded. Fig. 2 shows the representative Barrett–Joyner–Halenda (BJH) pore size distribution curves and adsorption–desorption isotherm plot (inset) of the TiO_2-NC and the TiO_2-NC hollow spheres calcined at 450 °C. The BJH method for calculating pore size distributions is based on a model of the adsorbent as a collection of cylindrical pores.[26] The method accounts for capillary condensation in the pores using the classical Kelvin equation[27]

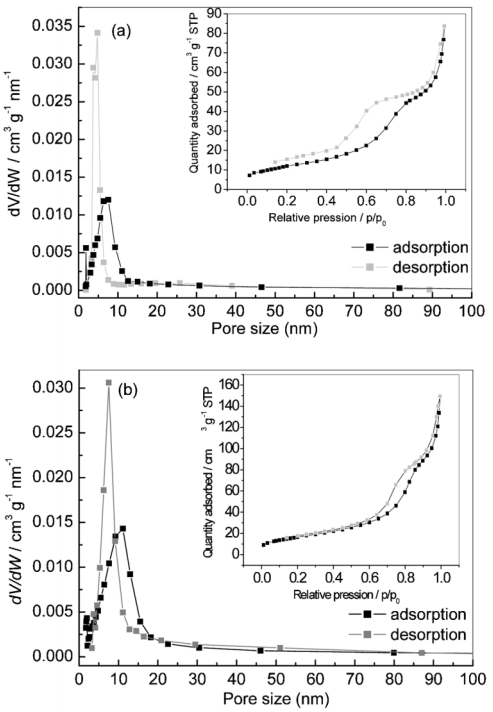

Fig. 2 The pore size distribution from the Barrett–Joyner–Halenda (BJH) method from both branches of the nitrogen adsorption/desorption isotherm (inset) of the TiO_2-NCs (a) and the TiO_2-NCs hollow spheres (b) calcined at 450 °C.

$$\ln\frac{p}{p^0} \geq \frac{-2\gamma V_L}{RT}\frac{1}{r_c}$$

where $r_c = \gamma - t(p)$ and r is the radius of the pore. V_L is the molar volume of the liquid, γ is the surface tension, and p^0 is the vapor pressure. The type of isotherm obtained with an inflection of nitrogen adsorbed volume at p/p^0 = 0.45 reveals the highly mesoporous nature of both synthesized samples. This observation was further confirmed by the mean pore diameter of 9 nm and 11.4 nm for the TiO_2-NC and the TiO_2-NC hollow spheres, respectively, which were obtained form the BJH pore size distribution (Fig. 2a and b). Based on the BJH method, the estimated error is usually less than 1%.[26,28] The main reason for the different pore size of the two samples is that a large number of channels were formed during the process of TiO_2-NC assembling into hollow spheres (as marked in Fig. 4c). These channels are expected to increase the surface area of materials, as well as improve the ionic and electronic charge transport, thus improving the performance of lithium storage in TiO_2, and this expectation is confirmed by the following tests. The determined Brunauer–Emmett–Teller (BET) surface area value was found to be 66.1 m^2 g^{-1} for the TiO_2-NC, but 91.6 m^2 g^{-1} for the TiO_2-NC hollow spheres, which again support the mesoporous nature and the presence of a large surface area due to the nanosized particles of TiO_2 and the ordered arrangement of the cone-like TiO_2. In this context, the surface area is a measure of the exposed active region of a solid available for electrochemical reaction. Whenever solid matter is divided into smaller particles, new surfaces are created, thereby increasing the total surface area. Similarly, when pores are created within the particle interior, the new surface area is also increased.

Fig. 3a and b show the typical FE-SEM and TEM images of the as-prepared TiO_2-NC. It can be seen that cone-like TiO_2 with a size of about 40–50 nm was formed during the LPD process and was self-organizing into a three-dimensional (3D) networks structure. It is expected that such a combination provides the electrode material with great porosity and thus improves the power density of the electrode *via* reducing the diffusion path length for ionic transport, which agrees well

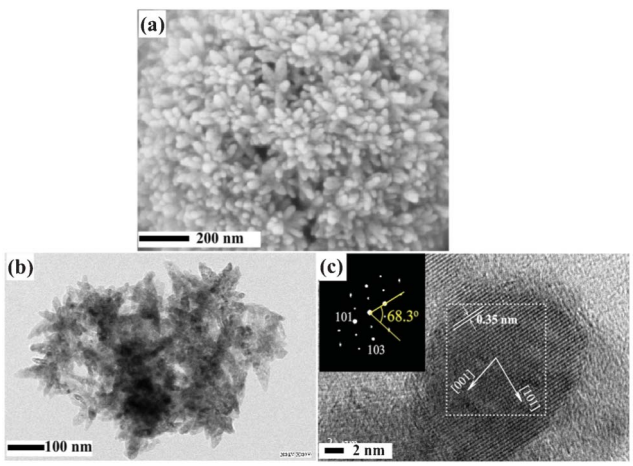

Fig. 3 FE-SEM (a), TEM (b) and HR-TEM (c) images of the TiO_2-NCs.

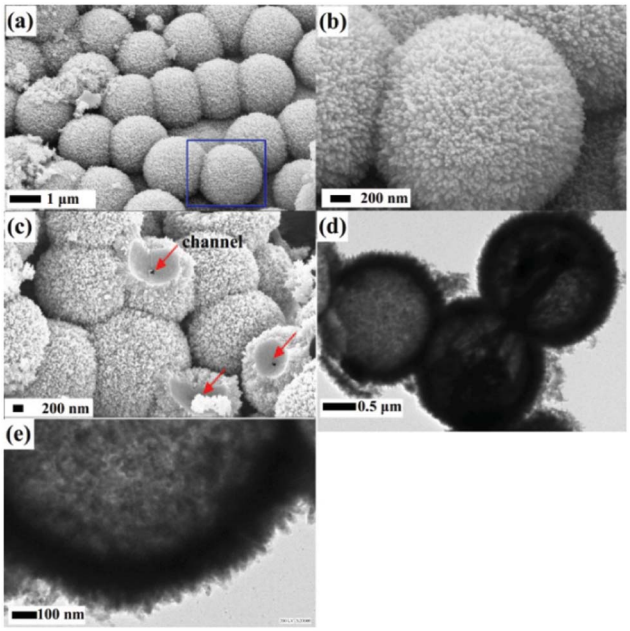

Fig. 4 FE-SEM (a, b, c), TEM (d) and high-magnification TEM (e) images of the TiO_2-NC hollow spheres.

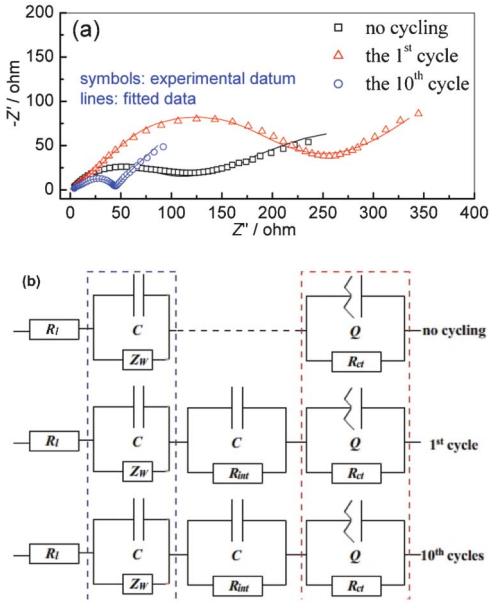

Fig. 5 Nyquist plots with fitted lines of the TiO_2-NCs at various cycles (a) and the corresponding equivalent circuits (b).

with the results of the BET test. The formation mechanism of the TiO_2-NC has been understood in our previous work.[4]

The high-resolution TEM (HR-TEM) image in Fig. 3c shows the anatase TiO_2 crystalline lattice fringes with an interplanar spacing of 0.35 nm, corresponding to anatase {101} facets. The XRD pattern (Fig. 1) also confirmed that the TiO_2-NC only contains anatase. Especially notable is the interfacial angle of 68.3° labeled in the corresponding fast-Fourier transform (FFT) pattern (Fig. 3c inset), which is identical to the theoretical value (68.3 ± 3°) for the angle between the {101} and {001} facets,[25] suggesting that the TiO_2-NC has exposed {001} facets on both the top and bottom of the nanocones. This preferred orientation is especially meaningful, because {001} facets possess superior Li storage capacity, as described in the introduction section.

Fig. 4 shows the FE-SEM and TEM images of the TiO_2-NC hollow spheres constructed by directly assembling the TiO_2-NC on the surface of the functionalized PS templates, which were removed by being dissolved in toluene. It can be seen from Fig. 4a and b that TiO_2 nanoparticles were assembled into well-defined spherical shells with a uniform and ordered arrangement. Moreover, the TiO_2 nanoparticles have the same morphology and size as the TiO_2-NC samples, meaning that the added supports (like PS) hardly affect the formation of cone-like TiO_2 in the LPD system. An especially notable fact is that cone-like TiO_2 particles were arranged more regularly in the hollow spheres than in the TiO_2-NC samples, and some channels (marked with red arrows in Fig. 4c) were formed among shells, which have the possibility to increase the surface area of the materials and to shorten the transmission path for the ion and electron. TEM images (Fig. 4d and e) clearly reveal the highly mesoporous nature of the spherical shells, which was confirmed by the BET test. In fact, the spherical shells were composed of a 3D network of cone-like TiO_2 with a wall thickness of about 300 nm. Such an arrangement can ensure a high uniformity of the material and provide enough channels for the diffusion of the electrolyte, which may help to enhance the utilization of the active area.

To better understand the kinetics of lithium storage in the cone-like TiO_2, we investigated the electrochemical impedance spectroscopy (EIS) of the TiO_2-NC samples, which was performed on an electrochemical system (Autolab PGSTAT 30, Ecochemie, The Netherlands) at the open circuit potential of the battery with frequencies from 10^5 to 10^{-1} Hz and the potential amplitude of 10 mV. Fig. 5 shows the Nyquist plots together with the modelling results and the corresponding equivalent circuits. In the equivalent circuit, R_l and R_{int} are associated with the resistance of electrolyte and interfacial films, respectively, and R_{ct} is the charge-transfer resistance reflecting the reactivity of lithium insertion/extraction in TiO_2. Z_W is the Warburg impedance representing the total resistance under the diffusion conditions. Table 1 presents the value of each element obtained from the fitting. An interesting result shown in Fig. 5b is the R_{int} element, which was absent in the no cycling but present in both the 1st and the 10th cycle. This

Table 1 Impedance parameters of the TiO_2-NCs electrode

	R_l/Ω	Z_W/Ω	R_{int}/Ω	R_{ct}/Ω
no cycling	2.15	893	—	69.5
the 1st cycle	2.54	80.6	4.2	173
the 10th cycle	3.77	57.2	4.6	37.1

result indicates that once the battery underwent charge/discharge cycles, some interfacial films would be formed. Herein the interfacial films may be caused by the formation of the solid electrolyte interphase (SEI) or the accommodation of lithium at the interfaces of the nanometer-sized particles. The former can result in an irreversible insertion of lithium into TiO_2, while the latter will contribute to an increased reversible capacity.[29] In fact, the SEI film is generally formed at low potentials (<1.0 V *vs.* Li^+/Li). In our cycling tests, the potential window is 1.5–2.5 V (*vs.* Li^+/Li), which hardly causes the decomposition of electrolyte to form the SEI films. Therefore, we infer that the bulk intercalation of lithium was accompanied by the phenomenon of interfacial storage in the TiO_2-NC. Another notable result shown in Fig. 5a is that, observing three cycles, the 1st cycle has the largest impedance semicycle, while the 10th cycle has the smallest one, indicating that the insertion reaction of lithium into TiO_2 is hard in the 1st cycle due to the laborious process of the initial diffusion and infiltration for the electrolyte in electrode materials. It can be seen from Table 1 that the electrode process is mainly controlled by diffusion steps (Z_W = 893 Ω) in the battery without being cycled. However, after the 1st cycle, the battery is characteristic of an electrode process mix controlled by diffusion (Z_W = 57.2 Ω) and charge-transfer (R_{ct} = 37.1 Ω) steps.[21] This result reveals the fact that the design of an anode material with a large area and channel structure is necessary and vital for the diffusion and insertion of lithium in TiO_2.

The Li-storage performance of both the TiO_2-NCs, and the TiO_2-NCs hollow spheres was evaluated. In general, Li insertion/extraction in anatase TiO_2 occurs according to the following equation:

$$TiO_2 + xLi^+ + xe^- = Li_xTiO_2\ (x \leqslant 1) \quad (1)$$

Among the polymorphs of titanium dioxide, the lithium insertion/extraction mechanism in the anatase phase has been most widely investigated. At x = 0.5, a structural phase transition from tetragonal TiO_2 to orthorhombic $Li_{0.5}TiO_2$ occurs. The theoretical capacity of anatase TiO_2 has been reported as 336 mA h g^{-1} (x = 1), while, for the fully reversible reaction, the maximum x is known to be 0.5, corresponding to a capacity of 168 mA h g^{-1}. At high lithium amounts in Li_xTiO_2 ($x > 0.5$), the reaction is known to become sluggish.[29] Cycling performances of the TiO_2-NC hollow spheres are shown in Fig. 6a, with the TiO_2-NC as a comparison. It is clearly observed in Fig. 6a that, at a rate of C/2 in the potential window of 1.5–2.5 V, the two samples exhibit excellent cyclic performances due to the inherent stability of TiO_2. It is notable that the two samples obtained high initial capacities. For the TiO_2-NC hollow spheres, the discharge capacity at the first cycle was 269.9 mA h g^{-1} (corresponding to $Li_{0.8}TiO_2$), and the first charge capacity delivered 250.1 mA h g^{-1}, corresponding to only a 7.3% initial capacity loss. The followed cycles exhibit significantly increased coulombic efficiency (almost to 100%) with a perfectly reversible capacity of 254.7 mA h g^{-1} (corresponding to $Li_{0.76}TiO_2$), which was preserved until the

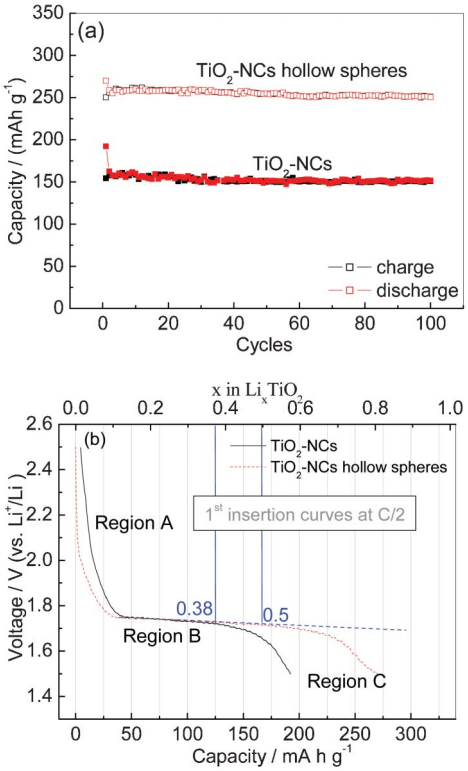

Fig. 6 Charge/discharge capacities *versus* number of cycles for the TiO_2-NCs and the TiO_2-NCs hollow spheres at rates of C/2 (a) and the corresponding voltage profiles during the first discharge process (b).

100th cycle with only very small capacity fading. For the TiO_2-NC sample, it has larger initial capacity loss, about 19.8%, but a high reversible capacity (152.9 mA h g^{-1}, $Li_{0.46}TiO_2$) can also be obtained. Thanks to the unique structure of cone-like TiO_2, such as exposed {001} facets and nanosized particles, our TiO_2-NC samples delivered higher reversible capacities than ordinary TiO_2 without cone-like features.[30] For the same features of cone-like TiO_2, the disordered and the systematic arrangement result in a low and a high specific surface area, respectively. High specific surface area helps to increase the diffusion of lithium ions in TiO_2, thus obtaining enhanced reversible capacity.

As shown in Fig. 6b, the discharge curves for the nanoporous anatase electrode can be divided into three different voltage regions, as reported in a previous study.[31] A monotonic voltage drop to ~1.75 V (~0.2 mol lithium insertion) occurs in the so-called region A. Region A is attributed to a homogeneous lithium insertion into the bulk, up to a solid-solution limit of lithium in TiO_2. After region A, a typical biphasic plateau (region B) is observed at a potential of ~1.75 V, where lithium-rich ($Li_{0.2}TiO_2/Li_{0.4}TiO_2$) phases are expected to coexist with the anatase phase (lithium-poor) TiO_2. After the biphasic plateau (region B), although more Li can be accommodated by further two-phase bulk intercalation ($x > 0.5$) at voltages over 1.75 V, the phases no longer reversibly dissolve lithium. However, further reversible storage of lithium

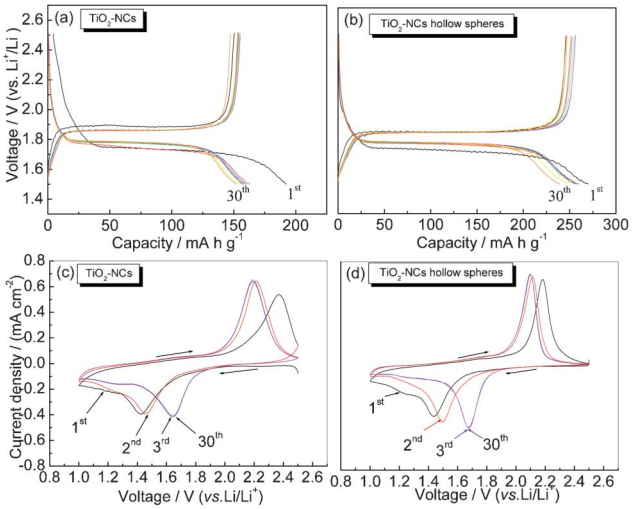

Fig. 7 Galvanostatic discharge (lithium-insertion)/charge (lithium-extraction) curves at rates of C/2 and cyclic voltammograms at a scanning rate of 0.2 mV s^{-1} for the TiO_2-NCs (a, c) and the TiO_2-NCs hollow spheres (b, d).

is able to occur at particle interfaces in this voltage region, representing region C.[32]

As discussed above, it is known that the main storage mechanism in anatase TiO_2 is the intercalation reaction (region A + B), based on eqn (1), in which lithium ions are randomly distributed over half of the available interstitial octahedral sites, leading to a theoretical capacity of 168 mA h g^{-1}. However, as the specific surface area increases, it has been reported that the proportion of region A + B decreases, while region C increases.[29] Discharge curves of the TiO_2-NC and the TiO_2-NC hollow spheres are displayed in Fig. 6b. When we compare the two geometrical arrangements of cone-like TiO_2, it is clear that ordered particles are indeed effective in improving both the bulk intercalation and the interfacial storage capacities, leading to an increase of region B (due to the shorter diffusion length) and C (due to the larger interfacial area). Therefore, based our case, we can conclude that an ordered arrangement for cone-like TiO_2 has an increased trend of lithium storage. Overvoltages that are already well visible in the region B plateau at the C/2 discharge, and also the low lithium content ($Li_{0.38}TiO_2$) at the end of region B further support a diffusion limit and thus a reduced electrochemically available volume for the TiO_2-NC sample. This is not the case for the TiO_2-NC hollow spheres sample. The end of the discharge plateau is close to the expected bulk limit with $Li_{0.5}TiO_2$ stoichiometry, indicating that, for the TiO_2-NC hollow spheres sample, the whole volume is available for electrochemical reactions.

Galvanostatic discharge/charge curves at rate of C/2 and cyclic voltammograms at a scanning rate of 0.2 mV s^{-1} for the TiO_2-NC and the TiO_2-NC hollow spheres are shown in Fig. 7. A notable difference in the voltage profiles was the plateau spacing, which reflects the degree of polarization of the electrode during the process of discharging/charging. Generally, the more serious polarization the electrode has,

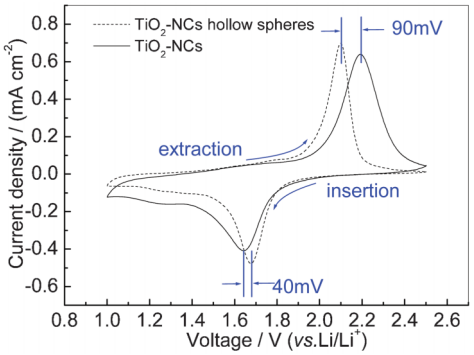

Fig. 8 The comparison of cyclic voltammograms for the TiO_2-NCs and the TiO_2-NCs hollow spheres.

the poorer performance exhibited by the materials. For the same anode material, a low potential of the discharge plateau and a high potential of the charge plateau mean a strenuous process for Li^+ insertion into TiO_2 and the lithium extraction from TiO_2. As shown in Fig. 7a and b, the discharge plateau potential of the TiO_2-NC is lower than that of the TiO_2-NC hollow spheres, while the charge plateau potential of the TiO_2-NC is higher than that of the TiO_2-NC hollow spheres. This result indicates that the lithium insertion/extraction was easier in the TiO_2-NC hollow spheres due to its ordered structure providing comfortable channels for the ionic and electronic diffusion. The cyclic voltammograms (Fig. 7c and d) show the same trend as the galvanostatic discharge/charge curves, that the performance of the TiO_2-NC hollow spheres sample is superior to the TiO_2-NC one. The striking differences in the cyclic voltammograms between the two samples are clearly displayed in Fig. 8. At the same scanning rate (0.2 mV s^{-1}), the TiO_2-NC hollow spheres sample has slightly larger redox peak currents (corresponding to lithium insertion/extraction peak currents). Noteworthy results shown in Fig. 8 are the different positions of the lithium insertion/extraction peak for the two samples. The potential of the Li^+ insertion peak is 1.68 V in the TiO_2-NC hollow spheres, more positive (40 mV) than that in the TiO_2-NC, and the potential of the lithium extraction peak is 2.2 V in the TiO_2-NC hollow spheres, more negative (90 mV) than that in the TiO_2-NC, showing significantly improved lithium-storage performance. This result agrees well with the conclusion of Fig. 6.

As a preferred sample, we investigated the rate performance of the TiO_2-NC hollow spheres. Normally, TiO_2 would be subject to rapid capacity decay at higher discharge/charge rates, such as in commercial TiO_2, while the TiO_2-NC hollow spheres performed very well. It can be seen from Fig. 9a that even at a high rate of 10 C, a higher reversible capacity, ~50 mA h g^{-1}, can also be delivered. In addition, the TiO_2-NC hollow spheres exhibited a better capacity retention of 97.7%, showing an excellent cycling performance. Generally, rapid ionic diffusion is necessary to obtain a high rate capability of LIB. Thus, the particularly high specific surface area with the large number of nanosized pores in the obtained, crystalline

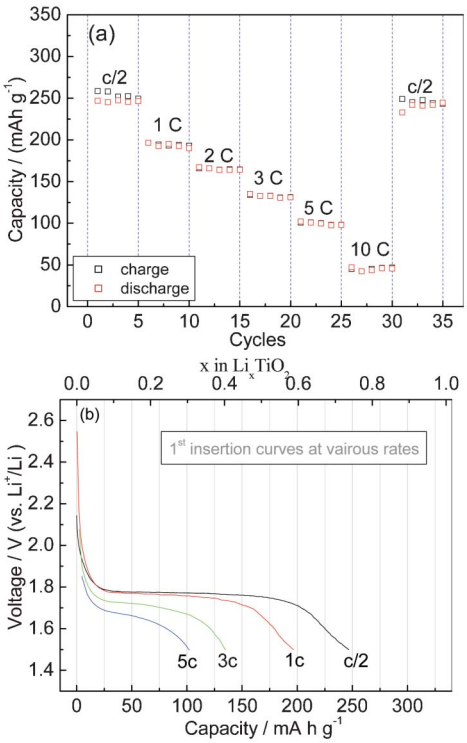

Fig. 9 Rate performance (a) and voltage profiles during the first discharge process (b) for the TiO_2-NCs hollow spheres.

anatase structure can significantly reduce the diffusion length for lithium ions, which contributes to the improved rate performance. Moreover, the substantially high surface area of the TiO_2-NC hollow spheres could provide many available extra sites for lithium accommodation at interfaces (interfacial storage),[32] beyond the fraction of octahedral sites available for the lithium-intercalation reaction in the bulk. Hence, a higher storage capacity can be obtained compared to nonporous materials. As mentioned in the reported literature,[33] one possible way of explaining the extra storage capacity is by the so-called 'job-sharing' mechanism. In this case, Li^+ would be stored in accessible interstitial sites at the oxide's side of the interface, while electrons would be stored in a second phase, such as carbon additives and SEI (solid electrolyte interphase) layers. Interfacial storage mechanisms could become especially important compared to the bulk intercalation mechanism in nanosized materials due to the high volume fraction of the interfacial regions.[32]

Fig. 9b presents the 1st insertion curves at various rates of the TiO_2-NC hollow spheres. In the 1st insertion cycle, the proportion of region C in the overall discharge capacity is about 35%, 50%, 65% and 80% at the discharge rates of C/2, 1C, 3C and 5C, respectively. Region C has a gradually increasing proportion of the overall discharge capacity as the discharge rate increases. This interesting result indicates that the reaction kinetics of an interfacial storage process are much faster than those of a bulk intercalation and phase change, and thus, high rates are able to provide more emphasis on the interface-based storage mechanisms. In this case, significantly higher charge/discharge rates could even prevent the bulk TiO_2 from being discharged above the $Li_{0.5}TiO_2$ threshold, where a part of any further bulk intercalation reactions could become irreversible. The material should then be subject to less degradation and capacity fading.

Conclusions

The structural properties and electrochemical behavior of TiO_2-NC have been investigated in detail in this paper to understand the contribution of the structure and the spatial arrangement of TiO_2-NC to lithium storage. The structural superiority of TiO_2-NC greatly helps to increase the surface area and shorten the diffusion lengths of ionic and electronic transport. In particular, the ordered arrangement of TiO_2-NC greatly enhances lithium storage, and delivered high reversible capacity (254.7 mA h g^{-1}). Moreover, electrochemical tests indicate that the bulk intercalation of lithium was accompanied by the phenomenon of interfacial lithium storage in TiO_2-NC. In addition, satisfactory rate performance can be achieved attribute to the 3D channels for the ionic and electronic diffusion in the TiO_2-NC hollow spheres. Another interesting result is that region C of the discharge curve has gradually increasing proportions of the overall discharge capacity as the discharge rate increases, indicating that the interfacial storage of lithium prefer the higher C-rate.

Acknowledgements

This work is supported by the joint project of National Natural Science Foundation of China and Natural Science Foundation of Guangdong Province (Grant No. U1134002), National Natural Science Foundation of China (Grant No. 21273084), Natural Science Fund of Guangdong Province (Grant No. 10351063101000001), and the key project of Guangdong Province (Grant No. 20110110).

Notes and references

1 S. W. Lee, B. M. Gallant, H. R. Byon, P. T. Hammond and Y. Shao-Horn, *Energy Environ. Sci.*, 2011, **4**, 1972.
2 C. K. Chan, H. Peng, G. Liu, K. McIlwrath, X. F. Zhang, R. A. Huggins and Y. Cui, *Nat. Nanotechnol.*, 2008, **3**, 31.
3 J. Chen, L. Xu, W. Li and X. Gou, *Adv. Mater.*, 2005, **17**, 582.
4 J. F. Lei, W. S. Li, X. P. Li and E. J. Cairns, *J. Mater. Chem.*, 2012, **22**, 22022.
5 D. Wang, D. Choi, J. Li, Z. Yang, Z. Nie, R. Kou, D. Hu, C. Wang, L. V. Saraf, J. Zhang, I. A. Aksay and J. Liu, *ACS Nano*, 2009, **3**, 907.
6 G. M. Bettez, T. R. Hawkins and A. H. Strømman, *Environ. Sci. Technol.*, 2011, **45**, 4548.
7 B. Scrosati, J. Hassoun and Y.-K. Sun, *Energy Environ. Sci.*, 2011, **4**, 3287.

8 N. Sata, K. Eberman, K. Eberl and J. Maier, *Nature*, 2000, **408**, 946.
9 J. Maier, *Solid State Ionics*, 2003, **157**, 327.
10 J. Maier, *Nat. Mater.*, 2005, **4**, 805.
11 Y. Yu, X. Wang, H. Sun and M. Ahmad, *RSC Adv.*, 2012, **2**, 7901.
12 D. Q. Zhang, G. S. Li, X. F. Yang and J. C. Yu, *Chem. Commun.*, 2009, 4381.
13 H. G. Yang, C. H. Sun, S. Z. Qiao, J. Zou, G. Liu, S. C. Smith, H. M. Cheng and G. Q. Lu, *Nature*, 2008, **453**, 638.
14 G. Liu, H. G. Yang, X. Wang, L. Cheng, J. Pan, G. Q. Lu and H. M. Cheng, *J. Am. Chem. Soc.*, 2009, **131**, 12868.
15 X. Xin, X. Zhou, J. Wu, X. Yao and Z. Liu, *ACS Nano*, 2012, **6**, 11035.
16 M. Liu, L. Piao, W. Lu, S. Ju, L. Zhao, C. Zhou, H. Li and W. Wang, *Nanoscale*, 2010, **2**, 1115.
17 E. Hosono, H. Matsuda, I. Honma, M. Ichihara and H. Zhou, *Langmuir*, 2007, **23**, 7447.
18 Y. W. Hu, T. Yang, X. X. Wang and K. Jiao, *Chem.–Eur. J.*, 2010, **16**, 1992.
19 X. Han, Q. Kuang, M. Jin, Z. Xie and L. Zheng, *J. Am. Chem. Soc.*, 2009, **131**, 3152.
20 Y. C. Qiu, K. Yan, S. H. Yang, L. M. Jin, H. Deng and W. S. Li, *ACS Nano*, 2010, **4**, 6515.
21 R. H. Zeng, X. P. Li, Y. C. Qiu, W. S. Li, J. Yi, D. S. Lu, C. L. Tan and M. Q. Xu, *Electrochem. Commun.*, 2010, **12**, 1253.
22 Y. G. Guo, Y. S. Hu, W. Sigle and J. Maier, *Adv. Mater.*, 2007, **19**, 2087.
23 M. Wagemaker, W. J. H. Borghols and F. M. Mulder, *J. Am. Chem. Soc.*, 2007, **129**, 4323.
24 H. K. Song, K. T. Lee, M. G. Kim, L. F. Nazar and J. Cho, *Adv. Funct. Mater.*, 2010, **20**, 3818.
25 G. Liu, C. H. Sun, H. G. Yang, S. C. Smith, L. Z. Wang, G. Q. Lu and H. M. Cheng, *Chem. Commun.*, 2010, **46**, 755.
26 M. L. Toebes, J. M. P. van Heeswijk, J. H. Bitter, A. J. van Dillen and K. P. de Jong, *Carbon*, 2004, **42**, 307.
27 L. D. Gelb and K. E. Gubbins, *Langmuir*, 1999, **15**, 305.
28 S. Bhattacharya and K. E. Gubbins, *Langmuir*, 2006, **22**, 7726.
29 J. Y. Shin, D. Samuelis and J. Maier, *Adv. Funct. Mater.*, 2011, **21**, 3464.
30 J. Yi, D. S. Lu, X. P. Li, S. J. Hu, W. S. Li, J. F. Lei and Y. Wang, *J. Solid State Electrochem.*, 2012, **16**, 443.
31 Y. G. Guo, Y. S. Hu and J. Maie, *Chem. Commun.*, 2006, 2783.
32 J. Y. Shin, D. Samuelis and J. Maier, *Adv. Funct. Mater.*, 2011, **21**, 3464.
33 Y. S. Hu, Y. G. Guo, R. Dominko, M. Gaberscek, J. Jamnik and J. Maier, *Adv. Mater.*, 2007, **19**, 1963.

